Threshold for primordial black holes: Dependence on the shape of the cosmological perturbations

Ilia Musco

▶ **To cite this version:**

Ilia Musco. Threshold for primordial black holes: Dependence on the shape of the cosmological perturbations. Physical Review D, 2019, 100 (12), pp.123524. 10.1103/PhysRevD.100.123524 . hal-01880815

HAL Id: hal-01880815
https://hal.science/hal-01880815

Submitted on 29 Jun 2023

HAL is a multi-disciplinary open access archive for the deposit and dissemination of scientific research documents, whether they are published or not. The documents may come from teaching and research institutions in France or abroad, or from public or private research centers.

L'archive ouverte pluridisciplinaire **HAL**, est destinée au dépôt et à la diffusion de documents scientifiques de niveau recherche, publiés ou non, émanant des établissements d'enseignement et de recherche français ou étrangers, des laboratoires publics ou privés.

Editors' Suggestion

Threshold for primordial black holes: Dependence on the shape of the cosmological perturbations

Ilia Musco*

Institut de Ciències del Cosmos, Universitat de Barcelona, Martí i Franquès 1, 08028 Barcelona, Spain;
Laboratoire Univers et Théories, UMR 8102 CNRS, Observatoire de Paris, Université Paris Diderot,
5 Place Jules Janssen, F-92190 Meudon, France,
and Département de Physique Théorique, Université de Genève,
24 quai E. Ansermet, CH-1211 Geneva, Switzerland

(Received 29 October 2019; published 16 December 2019)

Primordial black holes may have formed in the radiative era of the early Universe from the collapse of large enough amplitude perturbations of the metric. These correspond to non linear energy density perturbations characterized by an amplitude larger than a certain threshold, measured when the perturbations reenter the cosmological horizon. The process of primordial black hole formation is studied here within spherical symmetry, using the gradient expansion approximation in the long wavelength limit, where the pressure gradients are small, and the initial perturbations are functions only of a time-independent curvature profile. In this regime it is possible to understand how the threshold for primordial black hole formation depends on the shape of the initial energy density profile, clarifying the relation between local and averaged measures of the perturbation amplitude. Although there is no universal threshold for primordial black hole formation, the averaged mass excess of the perturbation depends on the amplitude of the energy density peak, and it is possible to formulate a well-defined criterion to establish when a cosmological perturbation is able to form a black hole in terms of one of these two key quantities. This gives understanding of how the abundance of primordial black holes depends on the shape of the inflationary power spectrum of cosmological perturbations.

DOI: 10.1103/PhysRevD.100.123524

I. INTRODUCTION

A population of primordial black holes (PBHs) might have been formed in the radiation dominated era of the early Universe, by gravitational collapse of sufficiently large-amplitude cosmological perturbations. This idea, suggested more than 50 years ago by Zel'dovich and Novikov in 1966 [1], was five years afterwards considered by Hawking [2]. Inspired by the fact that primordial black holes could be as small as elementary particles, by including semiclassical quantum corrections he discovered that a black hole could evaporate [3].

The cosmological consequences of PBH formation were then analyzed in more detail by Carr, Hawking's PhD student at that time, between 1974 and 1975 [4,5]. He formulated the first criterion to compute the threshold amplitude δ_c for PBH formation, using a simplified Jeans length argument in Newtonian gravity, obtaining $\delta_c \sim c_s^2$ where $c_s = \sqrt{1/3}$ is the sound speed of the cosmological radiation fluid measured in units of the speed of light. He was then followed by other authors who investigated the process of formation by gravitational collapse also numerically: Nadezhin, Novikov and Polnarev in 1978 [6]; Bicknell and Henriksen in 1979 [7]; Novikov and Polnarev in 1980 [8].

After these pioneering papers, progress on the mechanism of PBH formation was stalled for about 20 years until being studied again with more sophisticated numerical simulations by Niemeyer and Jedamzik [9] and Shibata and Sasaki [10], both in 1999, followed in 2002 by Hawke and Stewart [11], and by Musco, Miller and Rezzolla in 2005 [12]. PBH formation received a lot of attention at that time because of the discovery of critical collapse by Choptuik in 1993 [13]. This mechanism finds a natural application in the context of PBH formation, as pointed out in 1998 by Niemeyer and Jedamzik [14].

All of these numerical investigations confirmed that a cosmological perturbation is able to collapse to a PBH if it has an amplitude δ greater than a certain threshold value δ_c. One of the definitions of δ that can be found in the literature was introduced in [9], referring to the relative mass excess inside the overdense region (an averaged quantity) measured at the time of horizon crossing, when the radius of the cosmological horizon is exactly equal to the lengthscale of the overdensity measured in real space.

In [9] it was found that for a radiation fluid δ_c is between 0.67 and 0.71 depending on the shape of the energy density profile considered. Already at that time the issue of

*iliamusco@icc.ub.edu, ilia.musco@unige.ch

 © 2019 American Physical Society

measuring the lengthscale of the perturbation at the edge of the overdensity was arising when a non compensated perturbation, like the Gaussian shape with an overdensity spread to infinity, was considered. The problem was simply "solved" using a different prescription for measuring the lengthscale where the perturbation is characterized by a shape like the Gaussian, without investigating more deeply the issue of determining a well defined and unique criterion to measure the perturbation amplitude.

In [10] this was measured with the peak of the curvature profile (a local quantity) specified in Fourier space. Although these two papers came out in the same year, their approach, and the numerical techniques used, are very different and it was difficult at that time to compare the results obtained. The problem was confronted a few years later by Green *et al.* (2004) [15] using the relation between the curvature and the energy density profile known from the linear theory of cosmological perturbations, showing that the results of [10] corresponded to a value of δ_c varying between 0.3 and 0.5, which was not in agreement with the range of values obtained in [9].

There were two reasons for this. Firstly, as noted by Shibata and Sasaki in [10], the results of [9] had been contaminated by the inclusion of a decaying component which would have been absent in perturbations coming from inflation. This was rectified in our subsequent paper [12] where we obtained $\delta_c = 0.45$–0.47 for similar profile shapes to those in [9]. Since this was within the range of [15], $\delta_c = 0.45$ (for a Mexican-Hat perturbation) came to be used as a standard by cosmologists in many calculations of PBH formation. However, the measure of δ used in [15] is a local value of the energy density, while the amplitude measured in [9,12] is an averaged measure of the mass excess contained within the overdense region. Moreover the relation used in [15] is linear, while it was shown in [16] that the peak of the curvature profile forming a PBH needs to be at least of $O(1)$, which is obviously non linear. This inconsistency has long been under estimated, creating confusion in the literature and producing wrong estimates of the cosmological impact of PBHs, as Germani and myself have recently pointed out [17]. The same thing was noticed independently at the same time by Yoo *et al.* making a similar analysis [18].

One of the aims of the present paper is to combine together all of these aspects in a consistent and coherent picture, introducing a well defined criterion to measure the perturbation amplitude, which is shape independent. This clarifies the relation between the local and averaged measures of the perturbation amplitude, making it possible to compute consistently how the threshold for PBH formation varies with changing the shape of the initial density perturbation.

To do this I will follow the approach used in Polnarev and Musco (2007) [16], where supra horizon initial perturbations are described in terms of the non linear curvature profile, used to specify initial conditions for numerical simulations analogous to the ones performed in [12], using an asymptotic quasihomogeneous solution [19]. Because the curvature perturbation is a time-independent quantity when the perturbation lengthscale is much larger than the cosmological horizon [20], the initial perturbations for all of the other quantities can then be specified in a consistent way in terms of the initial curvature profile, even when this is non linear. This approach allowed Musco *et al.* [21] to show in 2009, implementing the previous numerical simulations with an adaptive mesh refinement (AMR), that the critical behavior continues to hold down to very small values of $(\delta - \delta_c)$. Finally in 2013 the self similarity of the solution for $\delta = \delta_c$ was analyzed and confirmed [22].

In 2014 Nakama *et al.* [23] made the first attempt to investigate the effects of the shape of cosmological perturbations on the threshold for PBH formation. They suggested two phenomenological parameters to measure the relation between the perturbation amplitude and the pressure gradients. Their analysis however only partially covers all of the possible range of shapes, and their phenomenological parameters cannot be easily related to the calculation of the cosmological impact of PBHs. The approach followed in this paper instead allows one to compute how δ_c and the corresponding peak amplitude of the energy density perturbations are varying with respect to the shape. This is perfectly consistent with peak theory [24] and shows that the abundance of PBHs is strongly dependent on the shape of the inflationary power spectrum, which determines the shape of the averaged perturbation collapsing to form PBHs [17].

For the work of this paper I have used the same numerical code as in our previous papers written on the subject. Following the present Introduction, Sec. II reviews the mathematical formulation of the problem, revising the quasihomogeneous solution and discussing the criterion to measure the perturbation amplitude, analyzing the relation between the local and averaged measures of the perturbation amplitude. In Sec. III different families of initial conditions are discussed, studying a wide range of perturbation profiles which allow identification of the fundamental properties of all possible shapes of the energy density. In Sec. IV the results for the threshold δ_c as a function of a fundamental parameter characterizing the shapes are presented and discussed. In Sec. V the conclusions are presented by making a summary of the results. Throughout we use $c = G = 1$.

II. MATHEMATICAL FORMULATION OF THE PROBLEM

A. Basics of the 3 + 1 ADM formalism

In general the $(3 + 1)$-decomposition of the metric in the Arnowitt-Deser-Misner (ADM) formalism [25,26] can be written as

$$ds^2 = -\alpha^2 dt^2 + \gamma_{ij}(dx^i + \beta^i dt)(dx^j + \beta^j dt), \quad (1)$$

where α, β^i and γ_{ij} are the lapse function, the shift vector and the spatial metric. In this $(3+1)$-decomposition, the unit timelike vector n_μ normal to the $t=$ const hypersurface Σ has the following covariant and controvariant forms:

$$n_\mu = (-\alpha, 0, 0, 0) \quad \text{and} \quad n^\mu = \left(\frac{1}{\alpha}, -\frac{\beta^i}{\alpha}\right). \tag{2}$$

In this paper I will consider matter described by a perfect fluid, with the stress energy tensor:

$$T^{\mu\nu} = (\rho + p)u^\mu u^\nu + pg^{\mu\nu}, \tag{3}$$

where ρ and p are the fluid energy density and the pressure measured in the comoving frame of the fluid, while u^μ is the four-velocity of the fluid normalized such that $u^\mu u_\mu = -1$. With these notions one can then write the $3+1$ Einstein equations for a perfect fluid in a general form without specifying a particular foliation of the space time (the *slicing*) and a particular family of worldlines (the *threading*). Choosing a particular combination of the two is equivalent to specifying the *gauge*. In general the spatial metric can be decomposed in the following form:

$$\gamma_{ij} = a^2(t)e^{2\zeta(t,x^i)}\tilde{\gamma}_{i,j}, \tag{4}$$

where $a(t)$ is the global scale factor and $\zeta(t, x^i)$ is a curvature perturbation describing the inhomogeneous Universe. The part of the three-metric given by $\tilde{\gamma}_{i,j}$ is time independent and such that $\det[\tilde{\gamma}_{i,j}] = 1$.

B. The long wavelength approach

We want to consider now non linear supra horizon perturbations with lengthscale much larger than the Hubble Horizon (which for a spatially flat Universe coincides with the cosmological Horizon). This approach has been variously called: long wavelength approximation [10], gradient expansion [27], anti-Newtonian approximation [28], and is based on expanding the exact solution as a power series in a fictitious parameter $\epsilon \ll 1$ that is conveniently identified with the ratio between the Hubble radius $1/H(t)$ [$H(t) \coloneqq \dot{a}(t)/a(t)$ is the Hubble parameter] which is the only geometrical scale in the homogeneous Universe, and the length scale L characterizing the perturbation.

$$\epsilon \coloneqq \frac{1}{H(t)L} \tag{5}$$

Choosing a particular value of ϵ corresponds to focusing on a particular value of time t, multiplying each spatial gradient by ϵ, expanding the equations in power series in ϵ up to the first non zero order and finally setting $\epsilon = 1$. This approach reproduces the time evolution of linear perturbation theory but also allows consideration of non linear curvature perturbations if the spacetime is sufficiently smooth for scales greater than L (see [20] and the references therein). This is equivalent to saying that pressure gradients are small when $\epsilon \ll 1$ and are not playing an important role in the evolution of the perturbation (we will come back to this later in Sec. II E).

We assume that $\zeta = 0$ somewhere in the Universe, which makes $a(t)$ the scale factor of that region, allowing us to interpret ζ as a perturbation within the observable Universe. In Fourier space the lengthscale L of the perturbation corresponds to a particular wave number $k \propto a(t)/L$ which allows ϵ to be expressed in terms of the wave number. This says that fixing the value of time t, the limit $\epsilon \to 0$ corresponds to $k \to 0$ and the Universe becomes locally homogeneous and isotropic (as in the Friedmann-Lemaître-Robertson-Walker (FLRW) solution) when the perturbation is smoothed out on a sufficiently large scale L.

The long wavelength approach is equivalent to the *separate Universe* hypothesis [29–31] which implies that it is always possible to find a coordinate system with which the metric of any local region can be written as

$$ds^2 = -dt^2 + a^2(t)\delta_{ij}dx^i dx^j, \tag{6}$$

where we have assumed the spatial flatness expected from inflation and confirmed by observations. While the homogeneous time-independent $\tilde{\gamma}_{ij}$ can be locally transformed away choosing the spatial coordinates, the time-dependent γ_{ij} cannot be homogeneous if we have a perturbation ζ which deviates our model of the Universe from the FLRW solution. It has been shown that in classical general relativity the $O(\epsilon)$ of $\dot{\tilde{\gamma}}_{ij}$ is decaying and therefore it is reasonable to assume $\dot{\tilde{\gamma}}_{ij} = O(\epsilon^2)$ while the shift component behaves as $\beta_i = O(\epsilon)$. This also implies that any perturbation ζ is time independent at the zero order in ϵ and $\dot{\zeta} = O(\epsilon^2)$, also for a non linear amplitude of ζ as it has been proved in [20].

C. The Misner-Sharp-Hernandez equations (comoving gauge)

Simulations of PBH formation have been performed by Shibata and Sasaki (S&S) [10] using the *constant mean curvature gauge*, characterized by a constant trace of the extrinsic curvature, while other groups (including ours) have been working using the *comoving gauge* which we are now going to specify. The relation between different gauges in the gradient expansion approximation has been analyzed extensively in [20,32].

In spherical symmetry the explicit form of the Einstein equations in the comoving gauge is known as the Misner-Sharp-Hernandez equations which start from the following diagonal form of the metric [33]:

$$ds^2 = -A^2(r,t)dt^2 + B^2(r,t)dr^2 + R^2(r,t)d\Omega^2, \tag{7}$$

where the radial coordinate r is taken to be comoving with the fluid, which then has the four-velocity of the fluid equal to the unit normal vector orthogonal to the hypersurface of constant time t, namely $u^\mu = n^\mu$, which is usually referred to as *cosmic time*. This metric corresponds to an orthogonal comoving foliation of the spacetime with the threading fixed by the shift vector $\beta^i = 0$. The non zero coefficients of the metric, A, B and R, are positive definite functions of r and t; R is called the *circumference coordinate* in [33] (being the proper circumference of a sphere with coordinate labels (r, t), divided by 2π) equivalent to the quantity referred to as the *areal radius*, and $d\Omega^2 = d\theta^2 + \sin^2\theta d\phi^2$ is the element of a 2-sphere of symmetry. The metric (7) can apply to any spherically symmetric spacetime; in the particular case of a homogeneous and isotropic universe it can be rewritten in the form of the FLRW metric given by

$$ds^2 = -dt^2 + a^2(t)\left[\frac{dr^2}{1 - Kr^2} + r^2 d\Omega^2\right], \tag{8}$$

with $K = 0, \pm 1$ being the spatial curvature for flat, closed and open Universes.

In the Misner-Sharp-Hernandez approach, two basic differential operators are introduced:

$$D_t \equiv \frac{1}{A}\frac{\partial}{\partial t} \quad \text{and} \quad D_r \equiv \frac{1}{B}\frac{\partial}{\partial r}, \tag{9}$$

representing derivatives with respect to proper time and radial proper distance in the comoving frame of the fluid. These operators are then applied to R, to define two additional quantities:

$$U \equiv D_t R = \frac{1}{A}\frac{\partial R}{\partial t} \quad \text{and} \quad \Gamma \equiv D_r R = \frac{1}{B}\frac{\partial R}{\partial r}, \tag{10}$$

with U being the radial component of four-velocity in an "Eulerian" (non comoving) frame where R is used as the radial coordinate, and Γ being a generalized Lorentz factor (which reduces to the standard one in the special relativistic limit). In other words U is measuring the velocity of the fluid with respect to the center of coordinates, that in the homogeneous and isotropic FLRW Universe is simply given by the Hubble law $U = HR$ with $R(r, t) = a(t)r$. The quantity Γ instead gives a measure of the spatial curvature, and in FLRW one gets $\Gamma^2 = 1 - Kr^2$. Note that Γ is just a constant ($\Gamma = 1$) when the Universe is homogeneous, isotropic and spatially flat.

In general U and Γ are related to the Misner-Sharp-Hernandez mass M (mathematically appearing as a first integral of the G^0_0 and G^1_0 components of the Einstein equations) by the *constraint equation*

$$\Gamma^2 = 1 + U^2 - \frac{2M}{R}, \tag{11}$$

where the interpretation of M as a mass becomes transparent when the form of the stress energy tensor, on the right hand side of the Einstein equations, is specified. Assuming a perfect fluid defined as in (3) M is given by

$$M = \int_0^R 4\pi R^2 \rho dR, \tag{12}$$

and in the FLRW Universe this integral is simply given by $M = 4\pi\rho_b(t)R^3/3$. In this case the constraint equation reduce to the First Friedmann equation

$$H^2(t) = \frac{8\pi}{3}\rho_b(t) - \frac{K}{a^2(t)}, \tag{13}$$

where $\rho_b(t)$ is the background energy density of the Universe.

The Misner-Sharp-Hernandez hydrodynamic equations obtained from the Einstein equations and the conservation of the stress energy tensor (see [33–35] for the details of the derivation) are:

$$D_t U = -\frac{\Gamma}{\rho + p} D_r p - \frac{M}{R^2} - 4\pi R p, \tag{14}$$

$$D_t \rho_0 = -\frac{\rho_0}{\Gamma R^2} D_r (R^2 U), \tag{15}$$

$$D_t \rho = \frac{\rho + p}{\rho_0} D_t \rho_0, \tag{16}$$

$$D_r A = -\frac{A}{\rho + p} D_r p, \tag{17}$$

$$D_r M = 4\pi R^2 \Gamma \rho, \tag{18}$$

where ρ_0 in Eqs. (15) and (16) is the rest mass density (or the compression factor for a fluid of particles without rest mass). Together with the constraint equation these form the basic set of the Misner-Sharp-Hernandez equations. Two other useful expressions coming from the Einstein equations are:

$$D_t \Gamma = -\frac{U}{e + p} D_r p, \tag{19}$$

$$D_t M = -4\pi R^2 U p. \tag{20}$$

To solve this set of equations we need one more equation to close the system, which is represented by the equation of state that is specifying the relation between pressure and the components of the energy density (see the Appendix).

In this paper I am going to consider a cosmological fluid with isotropic pressure described by

$$p = w\rho \tag{21}$$

with w constant. In particular $w = 0$ corresponds to a pressureless fluid (often referred to as "dust") while $w = 1/3$ corresponds to a radiation fluid.

D. The curvature profile

We can now introduce the curvature profile into the Misner-Sharp-Hernandez formulation of the Einstein equations as was done by Polnarev and Musco (P&M) [16], and subsequently also by Polnarev *et al.* [36] to study the formation of PBHs. In the comoving gauge this can be done conveniently using a function $K(r)$ replacing the constant curvature parameter of the FLRW metric (8) as

$$ds^2 = -dt^2 + a^2(t)\left[\frac{dr^2}{1-K(r)r^2} + r^2 d\Omega^2\right]. \tag{22}$$

Alternatively one can follow the standard approach used in cosmology keeping the curvature profile outside the spatial 3-metric as a perturbation of the scale factor, writing

$$ds^2 = -dt^2 + a^2(t)e^{2\zeta(\hat{r})}[d\hat{r}^2 + \hat{r}^2 d\Omega^2]. \tag{23}$$

In general the way of specifying the curvature profile into the metric fixes the parametrization of the radial comoving coordinate. Both (22) and (23) are asymptotic solutions of the Einstein equations in the limit of $t \to 0$ and the full solution is the *quasihomogeneous solution* described later in Sec. II E. The coordinate transformation between $K(r)$ and $\zeta(\hat{r})$ can be found by equating separately the radial and angular components of the two asymptotic metrics, obtaining as in [37]

$$\begin{cases} r = \hat{r}e^{\zeta(\hat{r})} \\ \frac{dr}{\sqrt{1-K(r)r^2}} = e^{\zeta(\hat{r})}d\hat{r}. \end{cases} \tag{24}$$

Harada *et al.* [32] contains an extensive discussion of the relation between the different gauges of the curvature profiles, with the aim of comparing the results for PBH formation obtained by P&M (using the *comoving gauge*) with the ones obtained by S&S (using the *constant mean curvature gauge*). In the long wavelength approximation the zero order of the curvature profile $\zeta(\hat{r})$ is gauge independent with differences arising at $O(\epsilon^2)$.

To connect directly $\zeta(\hat{r})$ to $K(r)$ one needs to insert the differential relation between $\hat{r}$ and r obtained from the first expression of (24),

$$\frac{dr}{d\hat{r}} = e^{\zeta(\hat{r})}(1 + \hat{r}\zeta'(\hat{r})), \tag{25}$$

into the second expression, which gives the following important relation:

$$\boxed{K(r)r^2 = -\hat{r}\zeta'(\hat{r})[2 + \hat{r}\zeta'(\hat{r})]} \tag{26}$$

already derived in [38] for a pressureless fluid. Another useful alternative relation can be obtained by comparing the time independent zero order component of the spatial curvature from the two asymptotic forms of the metric (22) and (23):

$$R^{(3)} = \begin{cases} \frac{2}{a^2(t)}\frac{1}{r^2}\frac{d}{dr}[r^3 K(r)] \\ -\frac{8}{a^2(t)}e^{-5\zeta(\hat{r})/2}\nabla^2 e^{\zeta(\hat{r})/2}, \end{cases} \tag{27}$$

which gives

$$\frac{d}{dr}[r^3 K(r)] = -\frac{4\hat{r}^2}{e^{\zeta(\hat{r})/2}}\nabla^2 e^{\zeta(\hat{r})/2}. \tag{28}$$

$\Psi(\hat{r}) \equiv e^{\zeta(\hat{r})/2}$ is the curvature profile as defined in S&S and the consistency of this expression with equation (26) can be verified using the transformation relations given by (24).

The relation between $K(r)$ and $\zeta(r)$ can also be found by using the definition of Γ given in (10) which is directly related to the curvature: at the zero order in ϵ one obtains

$$\Gamma^2 = 1 - K(r)r^2 = (1 + \hat{r}\zeta'(\hat{r}))^2, \tag{29}$$

which rearranged gives again (26). Note that for $K(r)r^2 = 1$ we have a coordinate singularity in the definition of metric (22) which can be solved with a coordinate transformation, as was pointed out in [39]. This point is distinguishing between PBHs of type I $[K(r)r^2 \leq 1]$ and PBHs of type II $[K(r)r^2 > 1]$ (see [40] for more details); however, the second case will not be considered here because, as we see in Sec. IV, the range of all possible values of the threshold δ_c is completely described by PBHs of Type I.

In general for any given profile $\zeta(\hat{r})$ one can compute the corresponding $K(r)$ by making the derivative of $\zeta(\hat{r})$ with respect to $\hat{r}$ and then changing the comoving radial coordinate with the first expression of (24). To obtain the inverse transformations from (29) we can write

$$d\zeta = \left(\sqrt{1-K(r)r^2} - 1\right)\frac{d\hat{r}}{\hat{r}} = \left(1 - \frac{1}{\sqrt{1-K(r)r^2}}\right)\frac{dr}{r},$$

where the second equality has been obtained using (24). As was shown in [32], this can then be integrated using the boundary condition at infinity where we assume for simplicity the Universe to be spatially flat

$$\lim_{r\to\infty} K(r)r^2 = 0 \qquad \lim_{\hat{r}\to\infty}\zeta(\hat{r}) = 0, \tag{30}$$

which finally gives

$$\begin{cases} \zeta(\hat{r}) = \int_\infty^r \left(1 - \frac{1}{\sqrt{1-K(r)r^2}}\right)\frac{dr}{r} \\ \hat{r} = r\exp\left[\int_\infty^r \left(\frac{1}{\sqrt{1-K(r)r^2}} - 1\right)\frac{dr}{r}\right]. \end{cases} \tag{31}$$

The solution of these integrals is not analytic, in general, and needs to be computed numerically.

E. The quasihomogeneous solution

In this subsection I am going to describe the explicit solution of the Misner-Sharp-Hernandez set of equations in the long wavelength approximation, as a function of the time independent curvature profile. The details of the derivation were presented in P&M using only $K(r)$; here I am going to review the main results presenting them also in terms of $\zeta(\hat{r})$ using the relations just seen above.

The time evolution of the scale factor and the Hubble parameter

$$a(t) \propto t^{\frac{2}{3(1+w)}} \quad \text{and} \quad H(t) \propto \frac{1}{t} \Rightarrow \epsilon \propto t^{\frac{1+3w}{3(1+w)}} \tag{32}$$

shows explicitly that choosing a particular value of ϵ with $k = \text{const}$ is equivalent to focusing on a particular value of time in the evolution of the perturbation. In particular for matter with $w > -1/3$ (like dust and radiation) the limit $\epsilon \to 0$ corresponds to $t \to 0$. As mentioned in Sec. II B the deviation from the asymptotic value of the metric tensor is $O(\epsilon^2)$, plus higher order terms that can be neglected when $\epsilon \ll 1$, and one can write the components of the cosmic time metric defined in (7) as

$$A = 1 + \epsilon^2\tilde{A} \tag{33}$$

$$B = \frac{R'}{\sqrt{1-K(r)r^2}}(1+\epsilon^2\tilde{B}) = a(t)e^{\zeta(\hat{r})}(1+\epsilon^2\tilde{B}) \tag{34}$$

$$R = a(t)r(1+\epsilon^2\tilde{R}) = a(t)e^{\zeta(\hat{r})}\hat{r}(1+\epsilon^2\tilde{R}), \tag{35}$$

and in the same way one can expand the hydrodynamical variables as

$$\rho = \rho_b(t)(1+\epsilon^2\tilde{\rho}) \tag{36}$$

$$U = H(t)R(1+\epsilon^2\tilde{U}) \tag{37}$$

$$M = \frac{4\pi}{3}\rho_b(t)R^3(1+\epsilon^2\tilde{M}), \tag{38}$$

where the pressure is then calculated with the equation of state given by Eq. (21). Putting R instead of $R_b = a(t)r$ outside the parenthesis in (37) and (38) simplifies the calculation allowing decomposition of the perturbation of M and U into the fundamental components.

Writing the constraint equation (11) as an expansion in ϵ, using its definition in Eq. (5), one gets

$$K(r) = a^2H^2\epsilon^2(\tilde{M} - 2\tilde{U}) \Rightarrow K(r)r_k^2 = \tilde{M} - 2\tilde{U}, \tag{39}$$

where r_k is the comoving lengthscale of the perturbation associated with the wave number k. Looking at this expression we can appreciate why in (37) and (38) it is useful to separate the perturbation of U and M from the perturbation of R. It also shows a general property of the quasihomogeneous solution: the profile of the perturbation is directly related to the curvature profile $K(r)$ or $\zeta(\hat{r})$, while the time evolution is governed by ϵ^2, with a clear separation between time and space dependence. Note that in the long wavelength approximation perturbations have the same time evolution as those in the linear theory for a pure growing mode.

The explicit expression for the energy density and velocity perturbations in terms of the curvature profile is then given by

$$\tilde{\rho} = \begin{cases} \frac{3(1+w)}{5+3w}\left[K(r) + \frac{r}{3}K'(r)\right]r_k^2 \\ -\frac{2(1+w)}{5+3w}\frac{e^{2\zeta(\hat{r}_k)}}{e^{2\zeta(\hat{r})}}\left[\zeta''(\hat{r}) + \zeta'(\hat{r})\left(\frac{2}{r} + \frac{1}{2}\zeta'(\hat{r})\right)\right]\hat{r}_k^2 \end{cases} \tag{40}$$

$$\tilde{U} = \begin{cases} -\frac{1}{5+3w}K(r)r_k^2 \\ \frac{1}{5+3w}\frac{e^{2\zeta(\hat{r}_k)}}{e^{2\zeta(\hat{r})}}\zeta'(\hat{r})\left[\frac{2}{\hat{r}} + \zeta'(\hat{r})\right]\hat{r}_k^2, \end{cases} \tag{41}$$

and note that, consistently with a pure growing solution, $\tilde{\rho}$ and $\tilde{U}$ can be expressed in terms of each other as

$$\tilde{\rho} = -(1+w)\frac{1}{r^2}\frac{d}{dr}(r^3\tilde{U}) \tag{42}$$

$$\tilde{U} = -\frac{1}{(1+w)}\frac{1}{r^3}\int \tilde{\rho}r^2dr. \tag{43}$$

To complete the solution one can write the other perturbation terms as linear combinations of energy density and velocity perturbations

$$\tilde{A} = -\frac{w}{1+w}\tilde{\rho} \tag{44}$$

$$\tilde{M} = -3(1+w)\tilde{U} \tag{45}$$

$$\tilde{R} = -\frac{w}{(1+3w)(1+w)}\tilde{\rho} + \frac{1}{1+3w}\tilde{U} \tag{46}$$

$$\tilde{B} = \frac{w}{(1+3w)(1+w)}r\frac{d\tilde{\rho}}{dr}, \tag{47}$$

where

$$r\frac{d}{dr}=\frac{\hat{r}}{1+\hat{r}\zeta'(\hat{r})}\frac{d}{d\hat{r}}.$$

Note that $\tilde{B}=0$ for $w=0$ and in general this term is related to pressure gradients which are responsible for the next order correction of $O(\epsilon^2)$ of the curvature profile, as can be appreciated from Eq. (19). One can look at $\tilde{B}$ as the seeds of pressure gradients which will grow during the non linear evolution, breaking the self similar behavior of the quasihomogeneous solution. It is also interesting to notice that the sum of the coefficients of $-2\tilde{U}$ and $\tilde{M}$ is equal to 1, because of the constraint equation written in terms of $K(r)$ seen in (39). The values of these coefficients show how the curvature perturbation splits between $\tilde{U}$ and $\tilde{M}$, with the two limits of pure kinetic energy for $w=-1$ and pure gravitational energy for $w\to\infty$.

To use the quasihomogeneous solution just derived one needs to specify the values of the background quantities: the energy density $\rho_b(t)$, the Hubble parameter $H(t)$ and the scale factor $a(t)$, related by the first Friedmann equation (13). These allow $\epsilon(t)$ to be written as

$$\epsilon(t)=\frac{1}{a(t)H(t)r_k}=\frac{1}{a(t)H(t)\hat{r}_k e^{\zeta(\hat{r}_k)}}, \tag{48}$$

which inserted into (36) and (37) gives

$$\frac{\delta\rho}{\rho_b}=\begin{cases}\left(\frac{1}{aH}\right)^2\frac{3(1+w)}{5+3w}\left[K(r)+\frac{r}{3}K'(r)\right]\\ -\left(\frac{1}{aH}\right)^2\frac{3(1+w)}{5+3w}e^{-2\zeta(\hat{r})}\left[\zeta''(\hat{r})+\zeta'(\hat{r})\left(\frac{2}{\hat{r}}+\frac{1}{2}\zeta'(\hat{r})\right)\right]\end{cases} \tag{49}$$

$$\frac{\delta U}{U_0}=\begin{cases}(\frac{1}{aH})^2\frac{1}{5+3w}K(r)\\ (\frac{1}{aH})^2\frac{1}{5+3w}e^{-2\zeta(\hat{r})}\zeta'(\hat{r})[\frac{2}{\hat{r}}+\zeta'(\hat{r})],\end{cases} \tag{50}$$

where $U_0=HR$ differs from the background value because it includes the perturbation in R. The above expression represents an alternative way of writing the quasihomogeneous solution, with r_k not appearing explicitly, showing that the solution is scale independent.

In general it is possible to distinguish between compensated and non compensated density profiles: the first ones are characterized by overdensity regions compensated by underdensity ones such that

$$\int_0^\infty 4\pi r^2\tilde{\rho}dr=0\Rightarrow\begin{cases}\lim_{r\to\infty}K(r)r^3=0\\ \lim_{\hat{r}\to\infty}\zeta(\hat{r})\hat{r}=0,\end{cases} \tag{51}$$

while non compensated perturbations are characterized by a curvature profile not satisfying this limit but still satisfying the condition $\Gamma>0$ from (29), which gives

$$K(r)<\frac{1}{r^2}\quad\text{and}\quad\zeta'(\hat{r})>-\frac{1}{\hat{r}}. \tag{52}$$

Summarizing the boundary conditions at infinity in terms of $K(r)$ these are given by

$$\lim_{r\to\infty}K(r)\sim\frac{1}{r^\alpha}\begin{cases}\alpha>3 & \text{compensated}\\ 2<\alpha\leq 3 & \text{non compensated,}\end{cases} \tag{53}$$

while in terms of $\zeta(\hat{r})$ these are

$$\lim_{\hat{r}\to\infty}\zeta(\hat{r})\sim\frac{1}{\hat{r}^\alpha}\begin{cases}\alpha>1 & \text{compensated}\\ 0<\alpha\leq 1 & \text{non compensated.}\end{cases} \tag{54}$$

We will see explicit examples of compensated and non compensated profiles in Sec. III where we will discuss different parametrizations of the curvature profile.

F. The perturbation amplitude δ

To conclude this Sec. I introduce a measure of the perturbation amplitude. Defining the averaged mass excess within a certain volume as

$$\delta(r,t):=\frac{1}{V}\int_0^R 4\pi R^2\frac{\rho-\rho_b}{\rho_b}dR, \tag{55}$$

where $V=\frac{4}{3}\pi R^3$, and using the expressions for ρ and R seen above in the long wavelength approximation at $O(\epsilon^2)$, one gets

$$\delta(r,t)=\frac{3}{r^3}\int_0^r\frac{\delta\rho}{\rho_b}r^2dr=\epsilon^2(t)f(w)K(r)r_k^2, \tag{56}$$

where

$$f(w)=\frac{3(1+w)}{5+3w}.$$

Using $\epsilon(t)$ in terms of r_k as in (48) allows (56) to be written as

$$\delta(r,t)=\epsilon^2(t)\tilde{M}(r)=\left(\frac{1}{aH}\right)^2 f(w)K(r), \tag{57}$$

which shows that $K(r)$ is directly measuring the averaged mass excess within a sphere of comoving radius r, with a "transfer coefficient" $f(w)$ depending on the equation of state.

If the perturbation has a central overdensity (underdensity) of comoving radius r_0 surrounded by an underdensity (overdensity), it has been common to identify r_k with the edge of the overdensity (underdensity) r_0 which is given by the location where $\delta\rho/\rho_b=0$, obtained by

$$\begin{cases} K(r_0) + \frac{r}{3} K'(r_0) = 0 \\ [e^{\zeta(\hat{r}_0)/2}]' + \frac{r_0}{2} [e^{\zeta(\hat{r}_0)/2}]'' = 0. \end{cases} \quad (58)$$

However, if $r_0 \to \infty$ we have $\delta \to 0$, coherently with the boundary condition at infinity of the curvature profile seen in (30) and with the fact that a perturbation with infinite lengthscale ($k \to 0$) is equivalent to the background solution. This shows that in general r_0 is not a good measure of the perturbation lengthscale and it is necessary to find an alternative way to quantify the perturbation amplitude.

One can define the compaction function $\mathcal{C}$, according to the $R = 2M$ condition for the formation of an apparent horizon,[1] as twice the mass excess over the areal radius

$$\mathcal{C} := \frac{2[M(r,t) - M_b(r,t)]}{R(r,t)} = \frac{r^2}{r_k^2} \tilde{M} + O(\epsilon^2), \quad (59)$$

where in the second equality we have used the first Friedmann equation (13) for a Universe which is spatially flat.[2] Neglecting the higher order terms in ϵ^2, consistently with the long wavelength approximation, one finds that $\mathcal{C}$ is time independent, and using the explicit expression for $\tilde{M}$ we have

$$\mathcal{C}(r) = f(w) K(r) r^2 = \frac{r^2}{r_k^2} \delta(r) \quad \Rightarrow \quad \mathcal{C}(r_k) = \delta(r_k), \quad (60)$$

where $\delta(r)$ is the spatial component of (55), i.e., $\delta(r,t) = \epsilon^2(t)\delta(r)$. This shows the equivalence of measuring the amplitude in terms of the excess of mass within a comoving volume of radius r_k or in terms of the local value of the compaction function. Because we are looking at PBH formation it is natural to identify r_k with the location r_m where $\mathcal{C}(r)$ is reaching its maximum, defined by $\mathcal{C}'(r) = 0$, which gives:

$$\begin{cases} K(r_m) + \frac{r_m}{2} K'(r_m) = 0 \\ \zeta'(\hat{r}_m) + \hat{r}_m \zeta''(\hat{r}_m) = 0. \end{cases} \quad (61)$$

Using these relations one can express $K'(r_m)$ in terms of $K(r_m)$, or $\zeta''(\hat{r}_m)$ in terms of $\zeta'(\hat{r}_m)$, and inserting these into (49), using also (57), we finally obtain

$$\boxed{\delta(r_m, t) = 3 \frac{\delta\rho(r_m, t)}{\rho_b(t)}} \quad (62)$$

which is completely independent of the particular shape of the curvature profile. This simple expression, which to my knowledge has never been pointed out before, shows the general relation between the local value of the energy density perturbation $\delta\rho/\rho_b$ measured at r_m and the averaged excess of mass δ within a comoving volume of radius r_m. The coefficient 3 is related to the spatial dimensions of the volume in spherical symmetry. Because of the "local to global" relation given by this expression, evaluating the energy density, or the mass excess at r_m, represents an invariant and well defined criterion to measure the amplitude of a cosmological perturbation on supra horizon scales, when the curvature profile is time independent. Inserting (62) into (56) one can write r_m as

$$r_m^3 = \frac{\int_0^{r_m} \delta\rho(r,t) r^2 dr}{\delta\rho(r_m, t)}, \quad (63)$$

which is an alternative definition of r_m using the energy density profile instead of the curvature. The location of r_m corresponds in general to the maximum of the Newtonian gravitational potential, measured by the ratio M/R.

To compare the amplitude of perturbations specified on different scales, it is useful to normalize $\epsilon = 1 \Rightarrow aHr_m = 1$, removing the time dependence from the expression for δ. In a first approximation this corresponds to the amplitude of the perturbation measured at horizon crossing (linearly extrapolated from the supra horizon regime), although a caveat is necessary here. In linear theory cosmological perturbations are usually described as single modes k evolving in the Fourier space and horizon crossing is defined as being when $k/aH = 1$.

Gravitational collapse forming a PBH instead is a non linear process happening in real space, where a perturbation is a combination of different modes over a region characterized by a particular lengthscale identified by location r_m of the maximum of $2M/R$. In the long wavelength regime, r_m will be associated with the "characteristic mode" k of the perturbation such that $r_m \propto 1/k$. In general the coefficient of proportionality between r_m and k depends on the particular curvature profile, which in Fourier space is associated with a particular shape of the inflationary power spectrum, and in [17] this connection has been computed for two particular shapes of the power spectrum, assuming Gaussian statistics.

The concept of horizon crossing therefore is not the same if measured in Fourier space or real space, and the non linear effects when $\epsilon \sim 1$ are not negligible (these will be analyzed in a future work). On the other hand extrapolating the horizon crossing from the quasihomogeneous solution putting $\epsilon = 1$ gives a reasonable estimation of the perturbation amplitude at horizon crossing and, most importantly, is a well defined criterion to compare different perturbations at the same scale r_m when computing the effect of the shape on the threshold for PBH formation.

In this context it is therefore useful to measure the amplitude of the perturbation at $\epsilon(t_H) \equiv 1$, which with an abuse of language I am going to call "horizon crossing time", defining

[1] See e.g., [41] for a review about the condition $R = 2M$ determining a trapped surface in spherical symmetry.

[2] This function was for the first time defined by S&S as $\mathcal{C} = (M - M_b)/R$.

$$\delta_m \equiv \delta(r_m, t_H) = f(w)K(r_m)r_m^2, \tag{64}$$

which in general will be different from the mass excess δ_0 measured at the edge r_0 of the overdensity

$$\delta_0 \equiv \delta(r_0, t_{H_0}) = f(w)K(r_0)r_0^2, \tag{65}$$

where t_{H_0} is the "horizon crossing time" defined with respect to r_0 instead of r_m. These expressions for $\mathcal{C}(r)$, δ_m and δ_0 can be expressed in terms of $\zeta(\hat{r})$ using (24) and (26).

III. INITIAL CONDITIONS

I am now going to study some specific parametrizations of the curvature profile $K(r)$ or $\zeta(\hat{r})$ to describe, using the quasihomogeneous solution seen in the previous section, different shapes as initial conditions for numerical simulations of PBH formation. I will start by considering an illustrative simple example of a Gaussian profile of $K(r)$ and $\zeta(\hat{r})$ containing only two parameters to vary: the amplitude and the length scale of the perturbation. This particular shape will then be generalized by introducing additional parameters, identifying which are the fundamental features characterizing the shape of the energy density.

A. Gaussian curvature profile

A Gaussian curvature profile for $K(r)$ is given by

$$K(r) = \mathcal{A}\exp\left(-\frac{r^2}{2\Delta^2}\right), \tag{66}$$

which inserted into (49) gives the following profile for the energy density:

$$\frac{\delta\rho}{\rho_b} = \left(\frac{1}{aH}\right)^2 f(w)\left[1 - \frac{r^2}{3\Delta^2}\right]K(r). \tag{67}$$

This type of perturbation is characterized by a central overdense region compensated by a surrounding underdense one approaching the background density at infinity, consistently with the condition seen in (53). The parameters $\mathcal{A}$ and Δ are controlling, respectively, the peak amplitude and the lengthscale of the perturbation. Using (61) and (58) we can calculate r_m and r_0 which allow computations of the values of δ_m and δ_0 defined in (64) and (65) as

$$r_m = \sqrt{2}\Delta \quad \Rightarrow \quad \delta_m = \frac{f(w)}{e}\mathcal{A}r_m^2 \tag{68}$$

$$r_0 = \sqrt{3}\Delta \quad \Rightarrow \quad \delta_0 = \frac{f(w)}{e^{3/2}}\mathcal{A}r_0^2. \tag{69}$$

Using (68) one can write (66) as a function of r/r_m

$$K(r) = \mathcal{A}\exp\left[-\left(\frac{r}{r_m}\right)^2\right], \tag{70}$$

which inserted into (67) gives

$$\frac{\delta\rho}{\rho_b} = \left(\frac{1}{aH}\right)^2 f(w)\left[1 - \frac{2}{3}\left(\frac{r}{r_m}\right)^2\right]K(r). \tag{71}$$

This is the so called *Mexican-Hat profile* of the energy density already used as an initial condition in [12]. When the Universe is radiation dominated ($w = 1/3$) a critical value of $\delta_0 \simeq 0.45$ was found, which corresponds to a critical value of $\delta_m \simeq 0.5$ and $\mathcal{A}r_m^2 \simeq 2$. In general we can relate the amplitude δ_m to the value of the peak measured at horizon crossing t_H ($\epsilon = 1$), obtaining

$$\frac{\delta\rho}{\rho_b}(0, t_H) = f(w)\mathcal{A}r_m^2 = e\delta_m. \tag{72}$$

The left frame of Fig. 1 shows the behavior of $K(r)$ as a function of r for three different choices of $\mathcal{A}$ and r_m^2 corresponding to the threshold $\delta_c \simeq 0.5$, where the dotted line corresponds to the condition $K(r)r^2 = 1$. In the right frame of Fig. 1 the corresponding profiles of the compaction function $C(r)$ are plotted, identifying the region of PBH formation with the amplitude of the peak corresponding to the threshold δ_c. Because $\mathcal{A} \propto 1/r_m^2$ for a constant value of δ_c, the different curves of Fig. 1 correspond to $C(r)$ written as a function of r/r_m, describing perturbations with the same amplitude δ_m specified at different scales.

Considering now a Gaussian curvature profile $\zeta(\hat{r})$ written in terms of $\hat{r}$ instead of r

$$\zeta(\hat{r}) = \mathcal{A}\exp\left(-\frac{\hat{r}^2}{2\Delta^2}\right), \tag{73}$$

one obtains the following energy density profile:

$$\frac{\delta\rho}{\rho_b} = \left(\frac{1}{aH}\right)^2 f(w)\left[1 - \frac{\hat{r}^2}{3\Delta^2}\left(1 + \frac{\zeta(\hat{r})}{2}\right)\right]\frac{2\zeta(\hat{r})}{\Delta^2 e^{2\zeta(\hat{r})}}. \tag{74}$$

Putting $\delta\rho/\rho_b = 0$ we have

$$\frac{\hat{r}_0^2}{3\Delta^2} = \left(1 + \frac{\zeta(\hat{r}_0)}{2}\right)^{-1}, \tag{75}$$

and the value of δ_0, the averaged amplitude measured at the edge of the overdensity, is given by

$$\delta_0 = -f(w)[2 + \hat{r}_0\zeta'(\hat{r}_0)]\hat{r}_0\zeta'(\hat{r}_0). \tag{76}$$

This shows that in general using $\zeta(\hat{r})$, the location of the edge of the overdensity, and the corresponding value of δ_0, depends both on $\mathcal{A}$ and Δ.

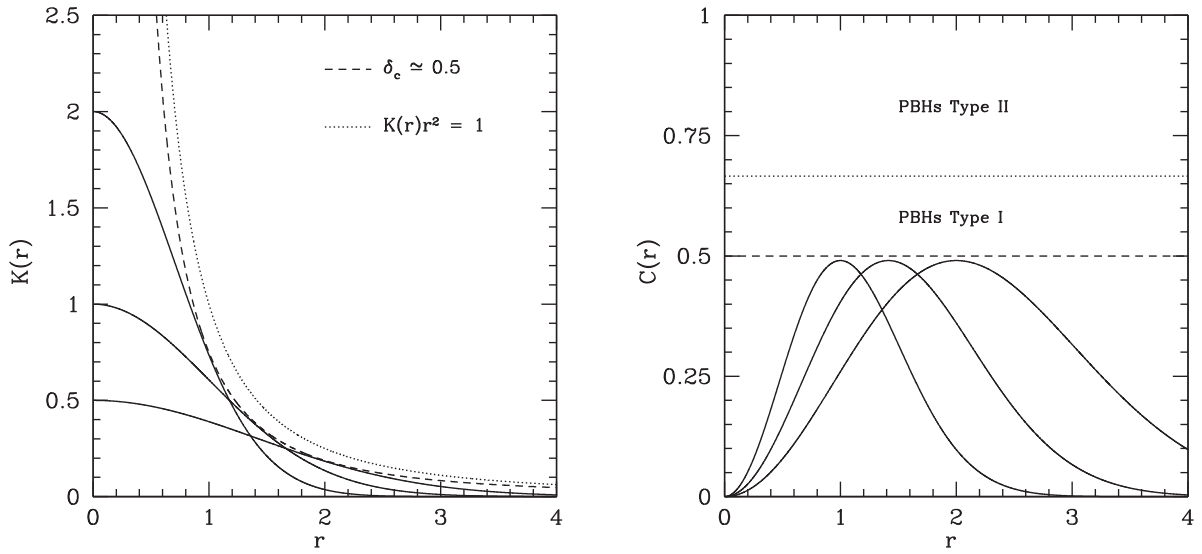

FIG. 1. The left plot shows the $K(r)$ given by (66) using the threshold value for PBH formation ($\delta_{m,c} \simeq 0.5$) for three different values of $r_m = 1, \sqrt{2}, 2$. The right plot shows the corresponding behavior of $\mathcal{C}(r)$ identifying 3 different parameter regions: no PBHs ($\delta_m \lesssim 0.5$), PBHs type I ($0.5 \lesssim \delta_m \leq 2/3$) and PBHs type II ($\delta_m > 2/3$).

Inserting (73) into the right hand expression of (61) one can calculate $\hat{r}_m$ as

$$\hat{r}_m = \sqrt{2}\Delta \quad \Rightarrow \quad \delta_m = 4f(w)\mathcal{A}e^{-1}(1-\mathcal{A}e^{-1}), \tag{77}$$

where δ_m depends only on the peak amplitude parameter $\mathcal{A}$, while the comoving lengthscale $\hat{r}_m$ of the perturbation depends only on Δ. The naturally split role of these two parameters confirms that the right choice is to measure the averaged excess of mass at $\hat{r}_m$ and not at $\hat{r}_0$. Equation (77) shows that there is a maximum value of δ_m for $\mathcal{A} = \mathcal{A}_{\max} = e/2 \simeq 1.36$, which corresponds to the coordinate singularity $K(r)r^2 = 1$. The threshold found for PBH formation using the Gaussian profile $\zeta(\hat{r})$ (73) rather than the Gaussian profile for $K(r)$ (66) gives a threshold $\delta_{m,c} \simeq 0.55$, corresponding to $\mathcal{A} \simeq 0.80$.

In the following I will generalize the shape of the curvature profile by introducing additional parameters to modify the shape of the energy density profile. Because the relation of $\delta\rho/\rho_b$ in terms of $K(r)$ is linear while the relation in terms of $\zeta(\hat{r})$ is not, in real space it is easier to control the shape working with $K(r)$ instead of $\zeta(\hat{r})$. The usage of $\zeta(\hat{r})$ becomes important when the profile in real space of the energy density is related to the power spectrum $\mathcal{P}_\zeta(k)$ in Fourier space obtained from inflation [17]. Because this paper is focusing on the relation between the threshold of PBH formation and the shape of cosmological perturbations collapsing to form PBHs in real space, I will focus only on different profiles of $K(r)$.

Numerical results obtained from different profiles of $\zeta(\hat{r})$ have instead been used in a related work [42] where the effects of the non linear relation between $\delta\rho/\rho_b$ and ζ on the cosmological abundance of PBHs have been investigated.

B. Compensated perturbation profiles

The Gaussian curvature profile seen in the previous subsection can be generalized by adding two additional parameters, α and λ, appearing as follows:

$$K(r) = \left(\frac{r}{\Delta}\right)^{2\lambda} \mathcal{A} \exp\left[-\frac{1}{2}\left(\frac{r}{\Delta}\right)^{2\alpha}\right], \tag{78}$$

which gives the following profile of the energy density:

$$\frac{\delta\rho}{\rho_b} = \left(\frac{1}{aH}\right)^2 f(w)\left[1 + \frac{2\lambda}{3} - \frac{\alpha}{3}\left(\frac{r}{\Delta}\right)^{2\alpha}\right] K(r). \tag{79}$$

Varying the first parameter $\alpha > 0$ changes the steepness of the profile, while varying $\lambda \geq 0$ changes also the location of the peak: for $\lambda = 0$ the peak is at the center ($r = 0$), while for $\lambda > 0$ the shape is off-centered and the distance between the peak and the center is increasing for larger values of λ.

The expressions for r_m and r_0 are given by

$$r_m = \left(\frac{2(\lambda+1)}{\alpha}\right)^{1/2\alpha} \Delta \tag{80}$$

$$r_0 = \left(\frac{2\lambda+3}{\alpha}\right)^{1/2\alpha} \Delta, \tag{81}$$

and the corresponding amplitudes δ_m and δ_0 are:

$$\delta_m = f(w)\left(\frac{2(\lambda+1)}{\alpha}\right)^{\lambda/\alpha} \exp\left(-\frac{\lambda+1}{\alpha}\right) \mathcal{A} r_m^2 \tag{82}$$

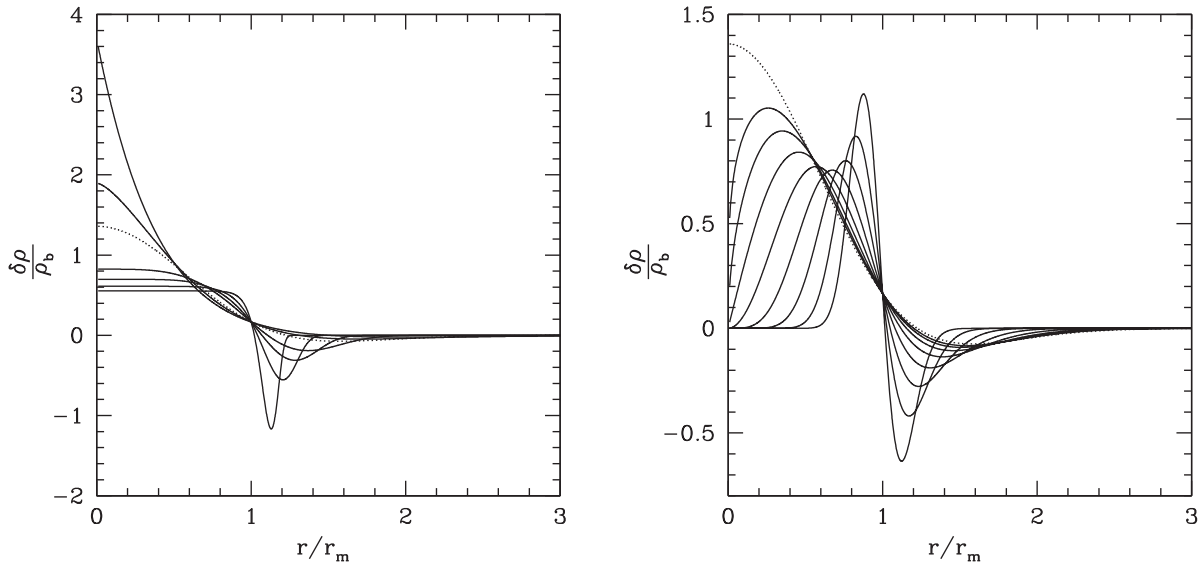

FIG. 2. This figure shows the behavior of $\delta\rho/\rho_b$ given by (85) plotted against r/r_m when $\epsilon = 1$. In the left frame the profiles are centrally peaked, with $\lambda = 0$ and $\alpha = 0.5, 0.75, 1, 2, 3, 5, 10$, while in the right one we can observe profiles which are off-centered, characterized by $\alpha = 1$ and $\lambda = 0, 1/8, 1/4, 1/2, 1, 2, 4, 8, 16$. In both frames the profile with $\alpha = 1$ and $\lambda = 0$ is plotted using a dotted line.

$$\delta_0 = f(w)\left(\frac{\lambda+3}{\alpha}\right)^{\lambda/\alpha}\exp\left(-\frac{2\lambda+3}{2\alpha}\right)\mathcal{A}r_m^2. \quad (83)$$

Using the value of r_m one can now rewrite (78) as

$$K(r) = (2\Lambda)^{\lambda/\alpha}\left(\frac{r}{r_m}\right)^{2\lambda}\mathcal{A}\exp\left[-\Lambda\left(\frac{r}{r_m}\right)^{2\alpha}\right], \quad (84)$$

where $\Lambda = (\lambda+1)/\alpha$, and (78) as

$$\frac{\delta\rho}{\rho_b} = \left(\frac{1}{aH}\right)^2 f(w)\left[1+\frac{2}{3}\lambda-\frac{2}{3}(\lambda+1)\left(\frac{r}{r_m}\right)^{2\alpha}\right]K(r). \quad (85)$$

The left frame of Fig. 2 shows the energy density contrast plotted against r/r_m for centrally peaked profiles ($\lambda = 0$) and different values of α, while in the right frame $\alpha = 1$ and λ is varying. The Mexican-Hat profile ($\alpha = 1$ and $\lambda = 0$) is plotted in both panels using a dotted line. In the left frame, the curves for $\alpha > 1$ have a lower peak than the Mexican Hat, while those for $\alpha < 1$ have a higher peak. For each profile $\delta_m = 0.5$ which implies that at $r = r_m$ the local value of the energy density $\delta\rho/\rho_b$ is the same, consistently with (62), and all of the different profiles are crossing each other at that point.

The region inside r_m in the left frame is getting more and more homogeneous for larger values of α while at the same time the transition to the background becomes sharper. For smaller values of $\alpha < 1$ the profiles become instead more spiky in the center while the transition towards the background solution outside becomes smoother.

The energy density profile can be characterized by the steepness of the profile, measured by r_0/r_m, which from (80) and (81) is given by

$$\frac{r_0}{r_m} = \left[\frac{2\lambda+3}{2(\lambda+1)}\right]^{1/2\alpha}. \quad (86)$$

Considering now a centrally peaked profile ($\lambda = 0$), the amplitude of the density peak $\delta\rho_0/\rho_b$ is related to the averaged amplitude δ_m as

$$\frac{\delta\rho_0}{\rho_b} = f(w)\mathcal{A}r_m^2 = e^{1/\alpha}\delta_m. \quad (87)$$

This shows that, for a constant value of δ_m, the corresponding value of the central density peak is decreasing for increasing values of α. This is reflecting the fact that for larger values of α the shape of $K(r)$ and $\delta\rho/\rho_b$ converges towards a top-hat profile with the matter becoming homogeneously distributed within a sphere of radius r_m. As shown also in [43], the parameter α is related to the width of the compaction function measured at r_m:

$$\alpha = -\frac{\mathcal{C}''(r_m)r_m^2}{4\delta_m}. \quad (88)$$

For a given lengthscale r_m and amplitude δ_m, when the peak of the energy density is sharp ($\alpha \ll 1$), the peak of the compaction function is broad, while when the peak of the energy density is broad ($\alpha \gg 1$), the peak of the compaction function is sharp. In the next section we are going to use this inverse behavior of the energy density

profile and the profile of the compaction function to show that the critical amplitude of the peak $(\delta\rho_0/\rho_b)_c$ is related to the threshold $\delta_{m,c}$. From now on these will be simply called $\delta\rho_c/\rho_b$ and δ_c.

C. Non compensated perturbation profiles

We next consider a generalization of the perturbation profiles analyzed previously adding an additional parameter that allows to decouple the behavior of the central region $(0 < r \leq r_m)$ from the tail of the perturbation $(r > r_m)$, taking into account also non compensated energy density perturbation profiles. For simplicity we start by considering a Gaussian shape of the energy density characterized by $(r_m/r_0) \to \infty$, given by

$$\frac{\delta\rho}{\rho_b} = \left(\frac{1}{aH}\right)^2 f(w)\mathcal{A}\left(\frac{r}{\Delta}\right)^n \exp\left[-\frac{1}{2}\left(\frac{r}{\Delta}\right)^2\right], \quad (89)$$

where the corresponding curvature profile $K(r)$ is obtained by performing the following integration:

$$K(r) = \frac{3aH}{r^3}\int_0^r \frac{\delta\rho}{\rho_b} x^2 dx^2. \quad (90)$$

We obtain an expression that, if n is an integer, can be written in the form of a series expansion:

(i) if n is even (90) gives

$$K(r) = 3\mathcal{A}\left(\frac{r}{\Delta}\right)^{-3}\left[B_n\sqrt{\frac{\pi}{2}}\mathrm{erf}\left(\frac{r}{\sqrt{2}\Delta}\right) - \sum_{i=0}^{n/2}\mathcal{C}_{\mathrm{in}}\left(\frac{r}{\Delta}\right)^{(n+1-2i)}\exp\left(-\frac{r^2}{2\Delta^2}\right)\right], \quad (91)$$

(ii) if n is odd (90) gives

$$K(r) = 3\mathcal{A}\left(\frac{r}{\Delta}\right)^{-3}\left[\mathcal{B}_n - \sum_{i=0}^{(n+1)/2}\mathcal{C}_{\mathrm{in}}\left(\frac{r}{\Delta}\right)^{(n+1-2i)} \times \exp\left(-\frac{r^2}{2\Delta^2}\right)\right], \quad (92)$$

where

$$\mathcal{B}_n = (n+1)!! \quad \text{and} \quad \mathcal{C}_{\mathrm{in}} = \frac{\mathcal{B}_n}{(n+1-2i)!!}.$$

In this case the value of r_m needs to be obtained by solving (61) numerically. The left frame of Fig. 3 shows different density profiles given by (89) for different values of n, all with the same amplitude $\delta_m = 0.5$, where the Gaussian shape with the peak in the center ($n = 0$) is plotted with a dashed line. The density profiles given by (89) are completely non compensated, without a region of underdensity, with n playing the same role of λ in the previous section.

These profiles can be generalized by introducing a varying compensation controlled by an additional parameter σ giving the energy density as

$$\frac{\delta\rho}{\rho_b} = \left(\frac{1}{aH}\right)^2 f(w)\mathcal{A}\left(\frac{r}{\Delta}\right)^n\left[\exp\left(-\frac{r^2}{2\Delta^2}\right) - \frac{1}{\sigma^3}\exp\left(-\frac{r^2}{2\sigma^2\Delta^2}\right)\right], \quad (93)$$

where $1 < \sigma < \infty$. This expression, using $n = 0$, was considered originally by S&S and corresponds to a Gaussian profile of the energy density modified by an underdensity which is more and more compensating the region of the overdensity for values of $\sigma \to 1$ while the opposite limit $\sigma \to \infty$ corresponds to (89). The parameter n is generalizing this behavior also for off-centered profiles. Inserting (93) into (90):

(i) for n even we have

$$K(r) = 3\mathcal{A}\left(\frac{r}{\Delta}\right)^{-3}\left[\mathcal{B}_n E1(r,\sigma) - \sum_{i=0}^{n/2}\mathcal{C}_{\mathrm{in}}\left(\frac{r}{\Delta}\right)^{(n+1-2i)}E2(r,\sigma)\right], \quad (94)$$

(ii) for n odd we have

$$K(r) = 3\mathcal{A}\left(\frac{r}{\Delta}\right)^{-3} \times \left[\mathcal{B}_n - \sum_{i=0}^{(n+1)/2}\mathcal{C}_{\mathrm{in}}\left(\frac{r}{\Delta}\right)^{(n+1-2i)}E2(r,\sigma)\right], \quad (95)$$

where

$$E1(r,\sigma) = \sqrt{\frac{\pi}{2}}\left[\mathrm{erf}\left(\frac{r}{\sqrt{2}\Delta}\right) - \mathrm{erf}\left(\frac{r}{\sqrt{2}\sigma\Delta}\right)\right] \quad \text{and}$$

$$E2(r,\sigma) = \exp\left(-\frac{r^2}{2\Delta^2}\right) - \frac{1}{\sigma}\exp\left(-\frac{r^2}{2\sigma^2\Delta^2}\right).$$

Imposing $\delta\rho/\rho_b = 0$ in (93) the following expression for r_0 is obtained:

$$\frac{r_0}{\Delta} = \sqrt{\frac{2(3+n)\sigma^2\log\sigma}{\sigma^2-1}}, \quad (96)$$

which is monotonically increasing for $1 < \sigma < \infty$. In the limit of $\sigma \to 1$ this expression gives $r_0 \to \sqrt{3}\Delta$: although for $\sigma = 1$ expression (93) reduces to the background solution, in the limit of $\sigma \to 1$ the shape converges to the "Mexican-Hat" profile analyzed in the previous section. The value of r_m for these shapes needs instead to be calculated numerically, then computing δ_m.

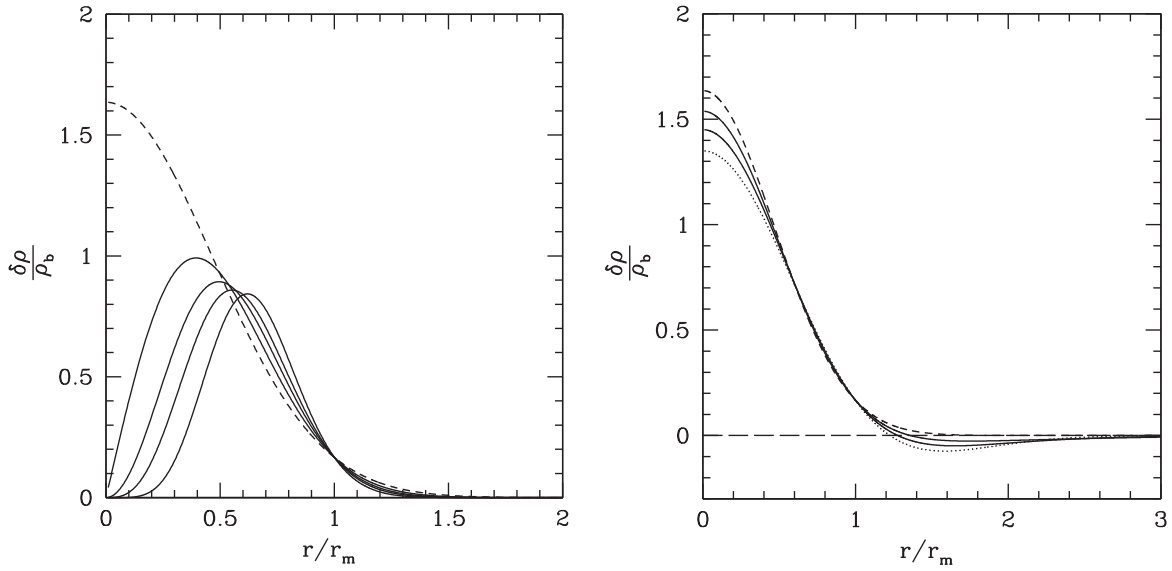

FIG. 3. This left panel here shows the behavior of $\delta\rho/\rho_b$ in (89) plotted against r/r_m at horizon crossing ($\epsilon = 1$) for $n = 0, 1, 2, 3, 5$. The right panel shows the behavior of $\delta\rho/\rho_b$ in (93) for $\sigma = 2, 3$ and for $\sigma \to \infty$. The Gaussian profile ($n = 0$ and $\sigma \to \infty$) in the left panel is plotted using a dashed line, while the Mexican-Hat profile ($\sigma \to 1$) is plotted in the right panel with a dotted line. In both panels all of the profiles correspond to a value of $\delta_m = 0.5$.

In the right frame of Fig. 3 the profiles given by (93) with $n = 0$ are plotted for different values of σ using a constant value of $\delta_m = 0.5$ for all of the profiles. As done in the left frame, the Gaussian profile ($n = 0$ and $\sigma \to \infty$) is plotted using a dashed line, while the Mexican-Hat profile ($\sigma \to 1$) is plotted with a dotted line. In principle it would be desirable to consider also a parameter α in the exponent of (93) changing the steepness of the profile, but this will introduce an additional level of complication in the integration of (90) which I will not consider in this context.

IV. THE THRESHOLD FOR PBH FORMATION

A. Numerical scheme

The calculations made in this paper to calculate the threshold of PBH formation for the different shapes described in the previous section have been made with the same code as used in [12,16,21,22]. This has been fully described previously and therefore just a very brief outline of it will be given here. It is an explicit Lagrangian hydrodynamics code with the grid designed for calculations in an expanding cosmological background. The basic grid uses logarithmic spacing in a mass-type comoving coordinate, allowing it to reach out to very large radii while giving finer resolution at small radii.

The initial data follow from the quasihomogeneous solution described in Sec. II, specified on a spacelike slice at constant initial cosmic time t_i with $a(t_i)r_m = 10R_H$ ($\epsilon = 10^{-1}$) while the outer edge of the grid has been placed at $90R_H$, sufficient to ensure that there is no causal contact between it and the perturbed region during the time of the calculations. The initial data is then evolved using the Misner-Sharp-Hernandez equations given in Sec. II C, so as to generate a second set of initial data on a null slice which is then evolved using the Hernandez-Misner equations (see [12]) for following the further evolution leading up to black hole formation. In this formulation, each outgoing null slice is labeled with a time coordinate u, which takes a constant value everywhere on the slice, and the formation of the apparent horizon is moved to $u \to \infty$, because of the increasing redshift of the null rays emitted by the collapsing shells.

During the evolution, the grid is modified with an adaptive mesh refinement scheme (AMR), built on top of the initial logarithmic grid, to provide sufficient resolution for following black hole formation down to extremely small values of $(\delta - \delta_c)$.

B. Shape parameters

In the previous section different types of profile have been analyzed, both compensated and not compensated, with the aim of having a wide variety of profiles so as to identify the key parameters describing the effects of the shape on the threshold for PBH formation. Based on this, we can now identify the minimum number of parameters describing the shape of the energy density to determine the threshold for PBH formation. As we will see later, the main features of the shapes are fixed by only one parameter, identified in the previous section with α, measuring the steepness of the shape, both of the energy density profile and of the compaction function.

In general any possible shape of the energy density perturbation is characterized by:

(i) The averaged mass excess δ_m contained within a spherical region of radius r_m, equivalent to measuring

the local value of the energy density perturbation $(\delta\rho/\rho_b)_{r_m}$, as shown by (62).

(ii) The peak amplitude of the energy density perturbation $(\delta\rho/\rho_b)_{r_p}$, located in general at $r_p \neq 0$.

(iii) The relative location r_p/r_m of the peak of the energy density; by definition $0 \leq (r_p/r_m) < 1$.

(iv) The relative location of the edge of the overdensity r_0/r_m; by definition $(r_0/r_m) \geq 1$.

In the plane of all possible profiles, $\delta\rho/\rho_b$ plotted against r/r_m, as presented in the previous section, these parameters identify 3 key points:

(i) $P_1 \coloneqq (r_p/r_m, (\delta\rho/\rho_b)_{r_p})$,
(ii) $P_2 \coloneqq (1, (\delta\rho/\rho_b)_{r_m})$,
(iii) $P_3 \coloneqq (r_0/r_m, 0)$.

If the profile is centrally peaked ($r_p = 0$) the behavior of the density will be basically monotonically decreasing from 0 to r_0, with the possibility of having only small oscillations so as not to alter the fact that r_m is the location of the peak of the compaction function. If the profile instead is not centrally peaked ($r_p \neq 0$), the behavior will be initially increasing from 0 to r_p and then decreasing from r_p to r_0.

The numerical results show that P_1, P_2 and P_3 contain all of the relevant information about the profile shape, and possible deviations are not playing any significant role during the non linear evolution. If the profile is not centrally peaked, we do not know in principle the value of $(\delta\rho/\rho_b)_{r=0}$. However, as we will see, during the evolution of an off-centered perturbation, the mass excess rearranges itself to a centrally peaked profile with almost the same value of the mass excess δ_m, which allows us to reduce the analysis to just centrally peaked profiles.

C. Numerical results

We start by considering the centrally peaked profiles given by (79), keeping $\lambda = 0$ and varying $\alpha > 0$. For $\alpha \to \infty$ the energy density profile approaches the top-hat profile characterized by an excess of mass homogeneously distributed from 0 to $r_0/r_m = 1$, with a discontinuous change of density to the background solution. For $\alpha \to 0$ the energy density profile instead approaches a Dirac-delta shape with $r_0/r_m \to \infty$.

For $\alpha \to \infty$ the profile of the compaction function converges towards a Dirac delta profile as indicated by (88) $[\mathcal{C}''(r_m) r_m^2 \to -\infty]$, while for $\alpha \to 0$ the compaction function converges towards a constant function $[\mathcal{C}''(r_m) r_m^2 = 0]$ like a top-hat profile. These are the asymptotic limiting cases, and between them one can find the typical Mexican-Hat shape characterized by $\alpha = 1$.

In the left frame of Fig. 4 one can see the behavior of the threshold δ_c calculated at r_m and the threshold $\delta_{0,c}$ calculated at the edge of the overdensity r_0, both plotted against r_0/r_m varying from 1 ($\alpha \to \infty$) to ∞ ($\alpha \to 0$). The two amplitudes diverge for increasing values of r_0/r_m with $\delta_{0,c} \to 0$ for $r_0/r_m \to \infty$ while δ_c is bounded by a minimum value ($\delta_{\min} \simeq 0.41$) for $r_0/r_m \to \infty$. Choosing δ_m instead of δ_0 to measure the amplitude of the overdensity minimizes the variation of the threshold, and should

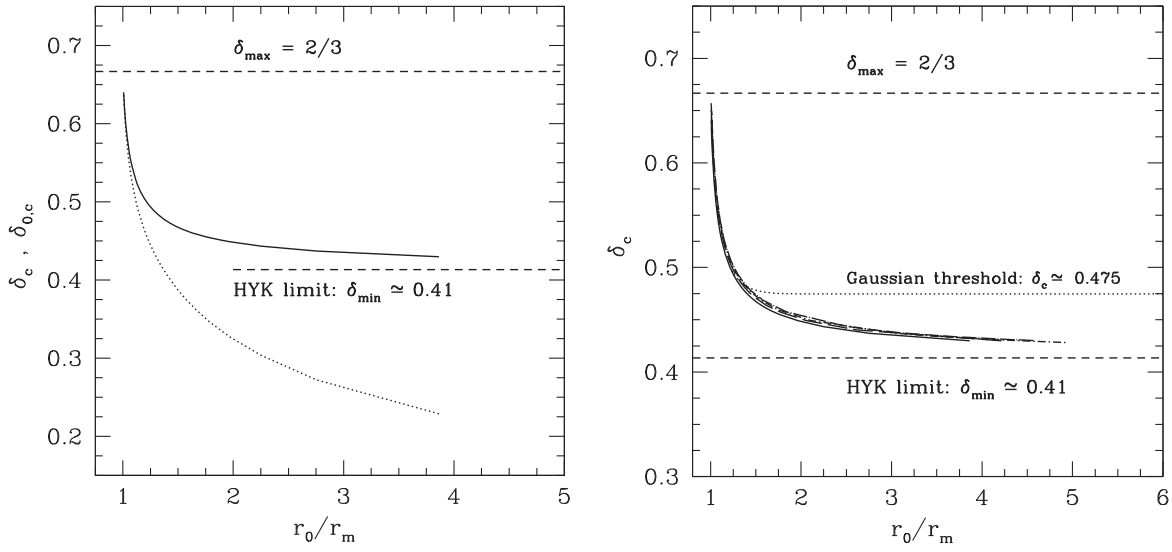

FIG. 4. The left panel shows the behavior of δ_c compared to the corresponding critical value $\delta_{0,c}$ plotted with respect to r_0/r_m for the centrally peaked profiles given by Eq. (79). The right panel shows the behavior of δ_c with respect to $(\delta\rho/\rho_b)_{r_p}$ for the profiles given by (79): the solid line corresponds to centrally peaked profiles ($\lambda = 0$) while the dashed lines correspond to off-centered profiles ($\lambda = 1$, 2, 3), with λ increasing and the behavior diverging from the solid line. The dotted line shows the behavior of the energy density profile given by (93) for $n = 0$ (centrally peaked) and σ varying from 1 to infinity. The two dashed horizontal lines represent the upper and lower boundaries for δ_c. as explained in the text. The lower bound is indicated with HYK from the names of the authors of [44], where this value was calculated.

therefore be preferred, also because of the shape independent property found at r_m, seen in (62).

The right frame of Fig. 4 shows δ_c plotted against r_0/r_m for both the centered and off-centered profiles given by (79), with $\lambda = 0$, 1, 2, 3 showing explicitly that the threshold δ_c does not change significantly between centered and off-centered profiles with the same steepness, measured here by r_0/r_m. The simulations show that during the first part of the evolution of the off-centered profiles, the matter is redistributing, filling up the central depression, converging towards a centrally peaked profile with almost the same amplitude that it would have had if it had been centrally peaked from the beginning. This suggests that the location of the peak of the energy density is not important, and that what mainly matters is the shape of the compaction function around the peak, which determines the value of the threshold δ_c. This allows simplification of the analysis considering only centrally peaked profiles for calculating the threshold δ_c and the corresponding critical value of the peak of the energy density $\delta\rho_c/\rho_b$, necessary to compute the cosmological abundance of PBHs [17,18] using peak theory [24].

The dotted line of Fig. 4 corresponds to the profiles given by Eq. (93) with $n = 0$ (centrally peaked) and varying σ from 1 to infinity. This gives a range of δ_c between 0.5 and 0.475 for $1 \leq r_0/r_m \lesssim 2$, while there is no significant variation in δ_c when $r_0/r_m \gtrsim 2$. The shape of these profiles changes significantly in the tail for $r \gtrsim r_m$, with a change of the central region $r \lesssim r_m$, corresponding to $\delta\rho_c/\rho_b$ varying between 1.35 and 1.55. The change in δ_c, varying between 0.41 and $2/3$ is therefore due to the variation of the shape in the central region of radius r_m, while keeping the same value of the peak of $\delta\rho/\rho_b$, only a few percent change is due to the shape in the region outside r_m, being completely negligible for $r \gtrsim 2r_m$.

The upper limit of $\delta_c = 2/3$, corresponds to the limit of validity of the comoving metric $[K(r_m)r_m^2 = 1]$, consistent with the discontinuity of the energy density profile at r_m. The lower limit $\delta_c \simeq 0.41$ is, instead, the analytic solution obtained for δ_c in [44] using a relativistic Jeans argument that takes into account the gravitational role of the pressure, but neglects pressure gradients, since otherwise no analytic solutions exist. All of this analysis suggests a general criterion to determine the threshold for PBH formation:

Proposition.—The value of the threshold for PBH formation is related to the role of the pressure gradients which depends on the shape around the peak of the compaction function, where the threshold is measured. A negligible role of the pressure gradients corresponds to a minimum value of the threshold (broad shape), while an infinite local value of the pressure gradients corresponds to the maximum value of the threshold (peaked shape).

In Fig. 5 one can see the monotonic inverse behavior of δ_c plotted against the corresponding critical peak value of the energy density perturbation $\delta\rho_c/\rho_b$, for centrally peaked profiles given by (79), with the following range of variation for these two quantities, linearly extrapolated from the supra horizon regime ($\epsilon = 1$):

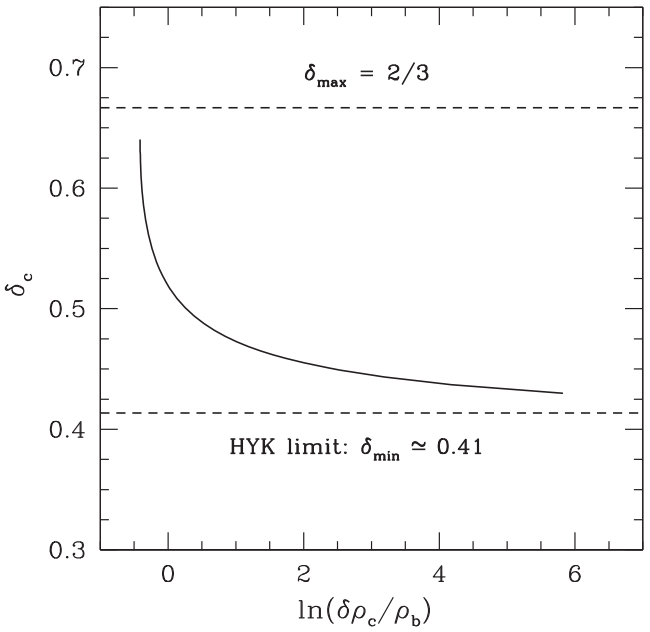

FIG. 5. This plot shows the variation of the threshold δ_c with respect to $\delta\rho_c/\rho_b$ for centrally peaked profiles given by Eq. (79) (solid line) and Eq. (93) (dotted line). The value of δ_c can vary between the two limiting cases indicated with the two dashed horizontal lines: the bottom one is the analytic limit computed in [44] when pressure gradients are negligible (Dirac-delta profile of the energy density), the upper one corresponds to the opposite case of infinite pressure gradients (top-hat profile of the energy density), and is converging towards the limit of validity of metric (7).

$$\boxed{\frac{\delta\rho_c}{\rho_b} \geq \frac{2}{3} \qquad 0.41 \lesssim \delta_c \leq \frac{2}{3}}. \tag{97}$$

The left side of Fig. 5 is consistent with an energy density profile converging towards a top-hat profile which has negligible pressure gradients in the center, and very large pressure gradients around r_m (minimum value of $\delta\rho_c/\rho_b = 2/3$ and a maximum value of $\delta_c = 2/3$). The very large pressure gradients at r_m for a top-hat profile of the energy density propagate inward modifying the profile very strongly during the non linear evolution, and this represents the shape which requires the largest amount of mass excess to compensate the effect of the pressure gradients at r_m in preventing the formation of a PBH.

The right side of Fig. 5 represents an energy density profile converging towards a Dirac-delta with very large pressure gradients in the center (maximum value of $\delta\rho_c/\rho_b \to \infty$) which corresponds to a compaction function around r_m converging to a constant behavior, implying negligible pressure gradients around r_m, and so giving a

minimum value of $\delta_c \simeq 0.41$. For such a matter configuration the pressure plays a significant role only in the very central region where almost all of the matter is already concentrated, while it is negligible through the rest of the configuration where the density in nearly constant.

When the perturbation is collapsing to a PBH ($\delta > \delta_c$), the difference between a particular value of δ_c and the minimum value of $\delta_c \simeq 0.41$ measures the additional excess of mass necessary to compensate the effects of the pressure gradients around r_m. The code is not able to evolve with good resolution shapes with $\alpha < 0.1$ because such profiles are too sharp, however the values of α considered allow for a very close approach to the analytic estimation of $\delta_c \simeq 0.41$ obtained in [44], called here the *HYK limit* from the names of the authors.

At the beginning of this section we identified 3 points characterizing the shape of the energy density. The analysis made here shows that these points are related to each other, and it is possible to use the family of curvature profiles given by

$$\frac{\delta\rho}{\rho_b} = \frac{\delta\rho_0}{\rho_b}\left[1 - \frac{2}{3}\left(\frac{r}{r_m}\right)^{2\alpha}\right]\exp\left[-\frac{1}{\alpha}\left(\frac{r}{r_m}\right)^{2\alpha}\right] \quad (98)$$

as a simple basis for energy density profiles to study the effect of the shape on the threshold, where this is well described by the single parameter α, measuring the width of the compaction function at the maximum r_m, renormalized with the amplitude of the perturbation measured at r_m [see (88)]. Knowing α one can compute the corresponding steepness of the profile r_0/r_m from (86), which neglecting off-centered profiles ($\lambda = 0$) gives

$$\frac{r_0}{r_m} = \left(\frac{3}{2}\right)^{1/2\alpha}. \quad (99)$$

Then from Fig. 4 one can compute the corresponding value of the threshold δ_c, neglecting the small correction coming from considering non compensated profiles, and then finally, from (87), compute the corresponding value of $\delta\rho_c/\rho_b$, as plotted in Fig. 5.

V. CONCLUSIONS

The threshold value of $\delta_{0,c} \simeq 0.45$ that was found in [12], corresponding to a Mexican-Hat shape, has been used for several years as a representative value for the threshold of PBH formation because it was consistent with the range $0.3 \lesssim \delta_c \lesssim 0.5$ calculated by Green *et al.* in [15]. This was obtained converting the results of the simulations done by S&S, that were using density profiles specified in the Fourier space, to a measure of the perturbation amplitude in real space.

There has been some confusion in the literature, with people using this value both for the threshold and for the critical amplitude of the peak, probably because it seemed that these two quantities should have roughly the same value. This however comes from using the linear approximation of (26), neglecting the term $(\nabla\zeta)^2$ which in simulations of PBH formation is not small, and approximating $e^{\zeta} \simeq 1 + \zeta$. These simplifications allow the density contrast in Fourier space to be written as

$$\frac{\delta\rho}{\rho_b}(k,t) \simeq -\left(\frac{k}{aH}\right)^2 \frac{2(1+w)}{5+3w}\zeta(k), \quad (100)$$

where $-k^2\zeta(k)$ is the Fourier transform of $\nabla^2\zeta(r)$.

However, considering the full non linear expression, it is not possible to simply transform the full expression for the energy density profile seen in (49) from the real space to the Fourier space. Also (100) is a local measure of the energy density profile while δ_m is an averaged smoothed quantity calculated within a volume of radius r_m. To follow a consistent approach it is necessary to identify the correct shape of the energy density profile starting from the shape of the power spectrum of cosmological perturbations. This can be done using the basis of profiles given by Eq. (98) of the previous section. This is a function only the single shape parameter α, characterizing the energy density profile.

According to the analysis in the previous section, with the value of the characteristic α it is possible to compute the corresponding value of the threshold δ_c and the critical peak amplitude $\delta\rho_c/\rho_b$, which needs to be used in peak theory [24] to compute the abundance of PBHs, with greater accuracy than using the Press-Schecther approach [17,18]. In a related work [45] it has been shown instead how to reconstruct the shape of the peak of the power spectrum of cosmological perturbations, starting from the numerical results obtained here using (98) as an initial condition, to obtain more accurate constraints on the amplitude of the peak of the power spectrum, assuming that PBHs account for all of the dark matter.

As we have seen previously, the expression for δ_m as a function of the curvature profile is given by

$$\delta_m = f(w)K(r_m)r_m^2 = -f(w)[2 + \hat{r}_m\zeta'(\hat{r}_m)]\hat{r}_m\zeta'(\hat{r}_m), \quad (101)$$

and we see that the fundamental quantity to measure is $\mathcal{K} \equiv K(r_m)r_m^2$ or $\Phi \equiv -\hat{r}_m\zeta'(\hat{r}_m)$, where the minus in the last expression is taken so as to make Φ positive. In terms of ζ the key quantity to measure is therefore its first derivative at r_m, multiplied by r_m to make the product adimensional. Considering the first derivative resolves the ambiguity that ζ could always be redefined by adding a constant, which corresponds to simply renormalizing the scale factor, or the radial Lagrangian coordinate, without changing the solution of the problem. Considering a radiation dominated Universe ($w = 1/3$), and inserting the range of δ_c given by (97) into δ_m given by (101), one obtains:

$$\boxed{0.62 \lesssim \mathcal{K}_c \leq 1 \qquad 0.38 \lesssim \Phi_c \leq 1}, \tag{102}$$

and Φ_c should replace the "misleading" concept of ζ_c that has been used in the literature for the curvature threshold of PBHs.

To summarize and conclude, in this paper a clear and consistent prescription has been given for calculating the perturbation amplitude δ_m of a spherically symmetric cosmological perturbation, measured at "horizon crossing", and then computing the threshold δ_c for PBH formation. A key point is to measure the density contrast at the location of maximum compactness, called here r_m, where the ratio $2M/R$ has a local maximum. Identifying r_m as the length-scale of the perturbation is justified by the fact that measuring the local value of the energy density at this point is equivalent to measuring the mass excess of the perturbation averaged within the corresponding volume, independently of the shape of the cosmological perturbation, as shown by (88).

This criterion enables one to understand how the shape of the perturbation affects the formation of PBHs: by performing extended numerical simulations, it has been shown here that the critical value of the peak amplitude of the energy density $\delta\rho_c/\rho_b$ is related to the value of δ_c, with a few percent variation due to the behavior of the "tail" of the profile in the region between r_m and $2r_m$. This analysis is valid also for off-centered profiles, because the dynamical evolution of these is equivalent to that of the centered ones with the same amplitude.

This analysis of the threshold for PBH formation has recently been used in [46] to study the possible effect on the threshold due to primordial non-Gaussianity of the power spectrum of cosmological perturbations.

ACKNOWLEDGMENTS

I. M. would like to thank Cristiano Germani, Jaume Garriga, Licia Verde, Nicola Bellomo, Pier Stefano Corasaniti, Tomohiro Harada, Chris Byrnes, Sam Young, Bernard Carr, Antonio Riotto, Alvise Racanelli, Alba Kalaja for useful discussion and suggestions concerning the content of this paper. I. M. is grateful to John Miller who has carefully checked the revised version of this paper, helping to improve the style of the presentation. I. M. would finally like to thank also Misao Sasaki for discussions during the YITP long-term workshop "Gravity and Cosmology 2018", YITP-T-17-02. I. M. is supported by the Unidad de Excelencia María de Maeztu Grant No. MDM-2014-0369, and from AGAUR 2014-SGR-1474.

Note added in the proof.—During the revision of this paper, in [43] it has been shown that, using the family of profiles given by (98), and computing the average of the compaction function within r_m, one obtains an averaged value of the threshold δ_c which is almost constant equal to 0.4, consistent with the HYK limit. This allows to derive an analytic relation to compute δ_c as a function of α (See Eq. (8) of [43]) with a few per cent deviation, consistent with the analysis presented in this section. This shows very clearly that the shape can be parameterized by only one parameter.

APPENDIX: PERFECT FLUID AND EQUATION OF STATE

The total energy density ρ is the sum of the rest mass density and the internal energy density:

$$\rho = \rho_0(1+e), \tag{A1}$$

where e is the specific internal energy, related to the velocity dispersion (temperature) of the fluid particles. In order to solve the set of equations presented in Sec. II we need to supply an equation of state $p(\rho_0, e)$ specifying the relation between the pressure and the different components of the energy density. For a simple ideal particle gas, we have that

$$p(\rho_0, e) = (\gamma - 1)\rho_0 e, \tag{A2}$$

where γ is the adiabatic index. In general, if $\gamma \neq 1$, Eq. (A1) can be written as

$$\rho = \rho_0 + \frac{p}{\gamma - 1} \tag{A3}$$

showing that, when the contribution of the rest mass of the particles to the total energy density is negligible ($\rho \gg \rho_0$, $e \gg 1$), we get the standard (one-parameter) equation of state used for a cosmological fluid

$$p = w\rho \tag{A4}$$

setting $w = \gamma - 1$. A pressureless fluid ($w = 0$) corresponds to the case where the specific internal energy ϵ is effectively zero, while $w = 1/3$ is appropriate for a radiation dominated fluid. In the case of Eq. (A4) the equation of state has a constant ratio of pressure over energy density given by w, while in general this ratio is varying with the density, increasing during the collapse. For an ideal gas in general we have

$$\frac{p}{\rho} = \frac{e}{1+e}(\gamma - 1), \tag{A5}$$

varying from $e(\gamma - 1)$ when $e \ll 1$ to the limit of w when $e \gg 1$.

[1] Ya. B. Zel'dovich and I. D. Novikov, Astron. Zh. **43**, 758 (1966); [Sov. Astron. **10**, 602 (1967)].
[2] S. W. Hawking, Mon. Not. R. Astron. Soc. **152**, 75 (1971).
[3] S. W. Hawking, Nature (London) **248**, 30 (1974).
[4] B. J. Carr and S. W. Hawking, Mon. Not. R. Astron. Soc. **168**, 399 (1974).
[5] B. J. Carr, Astrophys. J. **201**, 1 (1975).
[6] D. K. Nadezhin, I. D. Novikov, and A. G. Polnarev, Sov. Astron. **22**, 129 (1978).
[7] G. V. Bicknell and R. N. Henriksen, Astrophys. J. **232**, 670 (1979).
[8] I. D. Novikov and A. G. Polnarev, Sov. Astron. **24**, 147 (1980).
[9] K. Jedamzik and J. C. Niemeyer, Phys. Rev. D **59**, 124014 (1999).
[10] M. Shibata and M. Sasaki, Phys. Rev. D **60**, 084002 (1999).
[11] I. Hawke and J. M. Stewart, Classical Quantum Gravity **19**, 3687 (2002).
[12] I. Musco, J. C. Miller, and L. Rezzolla, Classical Quantum Gravity **22**, 1405 (2005).
[13] M. W. Choptuik, Phys. Rev. Lett. **70**, 9 (1993).
[14] J. C. Niemeyer and K. Jedamzik, Phys. Rev. Lett. **80**, 5481 (1998).
[15] A. M. Green, A. R. Liddle, K. A. Malik, and M. Sasaki, Phys. Rev. D **70**, 041502 (2004).
[16] A. G. Polnarev and I. Musco, Classical Quantum Gravity **24**, 1405 (2007).
[17] C. Germani and I. Musco, Phys. Rev. Lett. **122**, 141302 (2019).
[18] C. M. Yoo, T. Harada, J. Garriga, and K. Kohri, Prog. Theor. Exp. Phys. **2018**, 123E01 (2018).
[19] E. M. Lifshits and I. M. Khalamikov, Usp. Fiz. Nauk **80**, 391 (1963) [Sov. Phys. Usp. **6**, 496 (1964)].
[20] D. H. Lyth, K. A. Malik, and M. Sasaki, J. Cosmol. Astropart. Phys. 05 (2005) 004.
[21] I. Musco, J. C. Miller, and A. G. Polnarev, Classical Quantum Gravity **26**, 235001 (2009).
[22] I. Musco and J. C. Miller, Classical Quantum Gravity **30**, 145009 (2013).
[23] T. Nakama, T. Harada, A. G. Polnarev, and J. Yokoyama, J. Cosmol. Astropart. Phys. 01 (2014) 037.
[24] J. M. Bardeen, J. R. Bond, N. Kaiser, and A. S. Szalay, Astrophys. J. **304**, 15 (1986).
[25] R. Arnowitt, S. Deser, and C. Misner, Phys. Rev. **116**, 1322 (1959).
[26] R. Arnowitt, S. Deser, and C. Misner, Gen. Relativ. Gravit. **40**, 1997 (2008).
[27] D. S. Salopek and J. R. Bond, Phys. Rev. D **42**, 3936 (1990).
[28] K. Tomita, Prog. Theor. Phys. **54**, 730 (1975).
[29] M. Sasaki and T. Tanaka, Prog. Theor. Phys. **99**, 763 (1998).
[30] D. Wands, K. A. Malik, D. H. Lyth, and A. R. Liddle, Phys. Rev. D **62**, 043527 (2000).
[31] D. H. Lyth and D. Wands, Phys. Rev. D **68**, 103516 (2003).
[32] T. Harada, C. M. Yoo, T. Nakama, and Y. Koga, Phys. Rev. D **91**, 084057 (2015).
[33] C. W. Misner and D. H. Sharp, Phys. Rev. **136**, B571 (1964).
[34] W. C. Hernandez and C. W. Misner, Astrophys. J. **143**, 452 (1966).
[35] M. M. May and R. H. White, Phys. Rev. **141**, 1232 (1966).
[36] A. G. Polnarev, T. Nakama, and J. Yokoyama, J. Cosmol. Astropart. Phys. 09 (2012) 027.
[37] J. C. Hidalgo and A. G. Polnarev, Phys. Rev. D **79**, 044006 (2009).
[38] A. E. Romano, M. Sasaki, and A. A. Starobinsky, Eur. Phys. J. C **72**, 2242 (2012).
[39] M. Kopp, S. Hofmann, and J. Weller, Phys. Rev. D **83**, 124025 (2011).
[40] B. J. Carr and T. Harada, Phys. Rev. D **91**, 084048 (2015).
[41] A. Helou, I. Musco, and J. C. Miller, Classical Quantum Gravity **34**, 135012 (2017).
[42] S. Young, I. Musco, and C. T. Byrnes, J. Cosmol. Astropart. Phys. 11 (2019) 012.
[43] A. Escrivà, C. Germani, and R. K. Sheth, arXiv:1907.13311.
[44] T. Harada, C. M. Yoo, and K. Kohri, Phys. Rev. D **88**, 084051 (2013); **89**, 029903(E) (2014).
[45] A. Kalaja, N. Bellomo, N. Bartolo, D. Bertacca, S. Matarrese, I. Musco, A. Raccanelli, and L. Verde, J. Cosmol. Astropart. Phys. 10 (2019) 031.
[46] A. Kehagias, I. Musco, and A. Riotto, arXiv:1906.07135.